Organic Electronics 69 (2019) 174–180

Contents lists available at ScienceDirect

Organic Electronics

journal homepage: www.elsevier.com/locate/orgel

High V_{oc} ternary nonfullerene polymer solar cells with improved efficiency and good thermal stability

Zhen Wang, Yaowen Nian, Haiying Jiang, Feilong Pan, Zelong Hu, Lianjie Zhang, Yong Cao, Junwu Chen*

Institute of Polymer Optoelectronic Materials & Devices, State Key Laboratory of Luminescent Materials & Devices, South China University of Technology, Guangzhou, 510640, PR China

ARTICLE INFO

Keywords:
Polymer solar cells
Nonfullerene acceptor
2D/1a ternary blend
High open-circuit voltage
Thermal stability
Large area device

ABSTRACT

In this work, 2D/1A ternary blend films were designed based on two polymer donors of PTB7-Th and PBDB-T with comparable HOMO levels in combination with a nonfullerene O-IDTBR acceptor, which could display a high open-circuit voltage (V_{oc}) of 1.02 V. With an optimized blend of PTB7-Th:PBDB-T:O-IDTBR = 0.7:0.3:1.5, the ternary polymer solar cells (PSCs) showed PCEs of 11.58%, much higher than 9.74% and 6.99% for PTB7-Th:O-IDTBR and PBDB-T:O-IDTBR binary blend film, respectively. The improved efficiency for the ternary PSCs is due to the obviously elevated short-circuit current density. Higher charge dissociation probabilities, enhanced hole and electron transports, and favorable morphology were found for the ternary blend film. After long thermal annealing at 85 °C for 168 h, a good PCE of 9.37% was still retained by the ternary PSCs, remarkably higher than 5.33–6.27% for the two binary PSCs. In addition, the ternary PSCs with large areas of 0.37, 0.57, and 0.91 cm^2 were also evaluated, which displayed PCEs of 10.12%, 9.51%, and 9.01%, respectively. Our results demonstrated a high V_{oc} strategy for ternary PSCs, in which the efficiency and thermal stability could be optimized.

1. Introduction

Bulk heterojunction (BHJ) polymer solar cells (PSCs) have attracted considerable attention due to their advantages of light weight, flexibility, and low-cost potential via fast solution-processing [1–5]. Typically, the BHJ active layer of a PSC is composed by a donor material and an acceptor material. Currently, the performance of a fullerene acceptor based PSC is limited by some drawbacks of the fullerene, such as weak absorption in the visible region and hard tuning of the lowest unoccupied molecular orbital (LUMO) energy level [6]. To overcome the drawbacks of the fullerene acceptors, researchers have developed nonfullerene acceptors for PSCs [7–16]. So far nonfullerene based PSCs have shown higher power conversion efficiencies (PCEs) than the fullerene based PSCs, which are mainly attributed to enhanced light absorption, lower energy loss for exciton dissociation, and well controllable phase separation [17–19]. Recently, over 14% PCEs have been reported for the nonfullerene PSCs [20–23].

In general, an organic semiconducting material has a relatively narrow absorption window, which may limit photon harvesting by an active layer [24–26]. It has been demonstrated that a ternary blend is a simple and effective method that may improve photon harvesting for a higher short-circuit current (J_{sc}) if compared with a binary active layer [27–29]. So far, various complementary absorptions to solar irradiation have been demonstrated by ternary blend films, based on two donors blended with one acceptor (2D/1A) and one donor blended with two acceptors (1D/2A) [31,32].

For an organic active layer, the open-circuit voltage (V_{oc}) of a PSC strongly depends on the highest occupied molecular orbital (HOMO) level of the donor and the LUMO level of the acceptor [33–35]. There are several reports for binary PSCs with V_{oc} values higher than 1 V [36–41]. However, the V_{oc} values for most ternary systems are lower than one of their corresponding binary devices and very few of ternary PSCs can show V_{oc} over 1 V [42,43]. In a report by McCullouch et al. [43], a 1D/2A ternary blend based on PTB7-Th:IDTBR:IDFBR = 1:0.5:0.5 displayed a PCE of 11.0%, with a V_{oc} 1.03 V. Most ternary blends are selected based a strategy of cascade alignments for both HOMO and LUMO levels, which limits the maximizing of the V_{oc} despite the benefit for a higher J_{sc} [44–52].

In this work, we introduced a medium bandgap polymer PBDB-T to blend with narrow bandgap PTB7-Th:O-IDTBR binary system to fabricate a novel ternary PSC (Fig. 1). It should be noted that the HOMO level (E_{HOMO}) of PBDB-T of −5.28 eV is very close to the E_{HOMO} of

* Corresponding author.
E-mail address: psjwchen@scut.edu.cn (J. Chen).

https://doi.org/10.1016/j.orgel.2019.03.030
Received 24 February 2019; Received in revised form 16 March 2019; Accepted 16 March 2019
Available online 20 March 2019

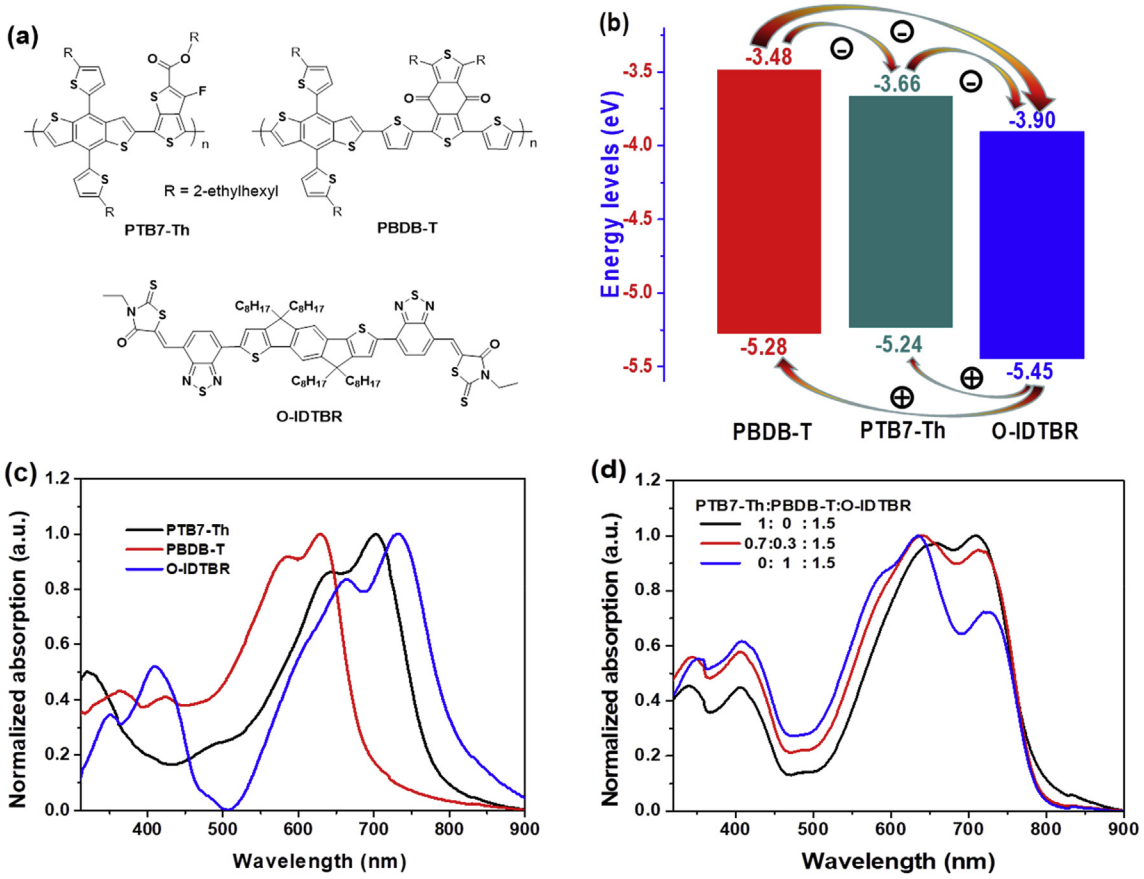

Fig. 1. (a) Chemical structures of polymer donors (PTB7-Th and PBDB-T) and non-fullerene accepter (O-IDTBR) in this work. (b) The corresponding energy level diagram related to the vacuum level. (c) Normalized UV–vis absorption spectra of PTB7-Th, PBDB-T, and O-IDTBR films. (d) Normalized UV–vis absorption spectra of PTB7-Th:O-IDTBR, PTB7-Th:PBDB-T:O-IDTBR, and PBDB-T:O-IDTBR blend films.

−5.24 eV for PTB7-Th (Fig. 1b) [17,53], so that the V_{oc} of the PTB7-Th:PBDB-T:O-IDTBR ternary PSCs can be maximized. Indeed, a V_{oc} of 1.02 V could be achieved for the 2D/1A ternary PSCs, which was one of the highest values among ternary PSCs. In addition, the ternary blend possesses cascade alignment of the LUMO levels as well as complementary absorption (Fig. 1c), two positive factors for a higher J_{sc}. Based on well controlled morphology, the PTB7-Th:PBDB-T:O-IDTBR ternary blends could exhibit significantly enhanced PCEs up to 11.58%, obviously higher than the 9.76% and 6.99% for the PTB7-Th:O-IDTBR and PBDB-T:O-IDTBR based binary blend films, respectively. Further thermal stability comparisons indicated that after 168 h thermal annealing at 85 °C in N_2 glove box, the ternary devices remained good PCEs of 9.37%, remarkably higher than the 6.27% and 5.33% for PTB7-Th:O-IDTBR and PBDB-T:O-IDTBR, respectively. Moreover, the photovoltaic performances of the ternary PSCs with different device areas of 0.057, 0.37, 0.57, and 0.91 cm^2 were also compared.

2. Results and discussions

The chemical structures of PTB7-Th, PBDB-T, and O-IDTBR are shown in Fig. 1a. Polymers PTB7-Th and PBDB-T, all comprising the same alkylthienyl substituted benzodithiophene (BDT) moiety, may possess good compatibility. To verify the fact, we calculated surface energies of PTB7-Th, PBDB-T, and PTB7-Th:PBDB-T (0.7:0.3) films, according to the Wu model [54]. As shown in Fig. S1, the water contact angles of PTB7-Th, PBDB-T, and PTB7-Th:PBDB-T (0.7:0.3) are of 94.0°, 97.5°, and 96.3°, respectively, while their contact angles to organic liquid CH_2I_2 are of 48.0°, 50.5°, and 48.7°, respectively (Table S1). The calculated surface energies for PTB7-Th and PBDB-T are comparable of 37.4 and 35.7 mJ/m^2, respectively. The PTB7-Th:PBDB-T blend film displays an intermediate surface energy of 36.5 mJ/m^2, suggesting good compatibility between the two polymer donors.

The HOMO energy levels (Fig. 1b) of PTB7-Th and PBDB-T are comparable of −5.24 and −5.28 eV, respectively, while PBDB-T, PTB7-Th, and O-IDTBR can establish cascade alignment of the LUMO levels. UV–vis absorption spectra of pristine films of PTB7-Th, PBDB-T, and O-IDTBR are shown in Fig. 1c. The maximum absorption of PTB7-Th locates at 696 nm, very close to that of 742 nm for O-IDTBR. Their absorption edges are at 776 and 815 nm, respectively, corresponding to optical bandgaps ($E_{g\text{-}opt}$) of 1.60 and 1.52 eV, respectively. Relatively, PBDB-T is a wider bandgap polymer ($E_{g\text{-}opt}$ = 1.78 eV) with a main absorption peak at 629 nm. Therefore, the two polymer donors PTB7-Th and PBDB-T can show a complementary absorption, which is beneficial for J_{sc} of the PSCs. Fig. 1d shows the absorption spectra of PTB7-Th:O-IDTBR, PBDB-T:O-IDTBR, and PTB7-Th:PBDB-T:O-IDTBR (0.7:0.3:1.5) blend films, based on a fixed D:A weight ratio of 1:1.5. For the absorption spectrum of PTB7-Th:O-IDTBR binary blend film, there are two strong absorption peaks at 655 and 710 nm but with a weak absorption band in the short-wavelength range (< 550 nm). The PBDB-T:O-IDTBR binary blend film exhibits a strong absorption peak at 635 nm and a weak shoulder at 723 nm, with relatively enhanced absorption from 320 to 635 nm and then decreased absorption in the longer wavelengths. For the PTB7-Th:PBDB-T:O-IDTBR (0.7:0.3:1.5), the ternary blend film displays a main peak at 642 nm and an enhanced shoulder peak at 717 nm. Generally, the ternary blend film can show a complementary absorption based on the two binary blend films. Generally, the absorption spectrum of the PTB7-Th:PBDB-T:O-IDTBR (0.7:0.3:1.5) ternary blend film corresponds to the absorption combination of the two binary blend films.

Bulk-heterojunction solar cells were fabricated in a conventional

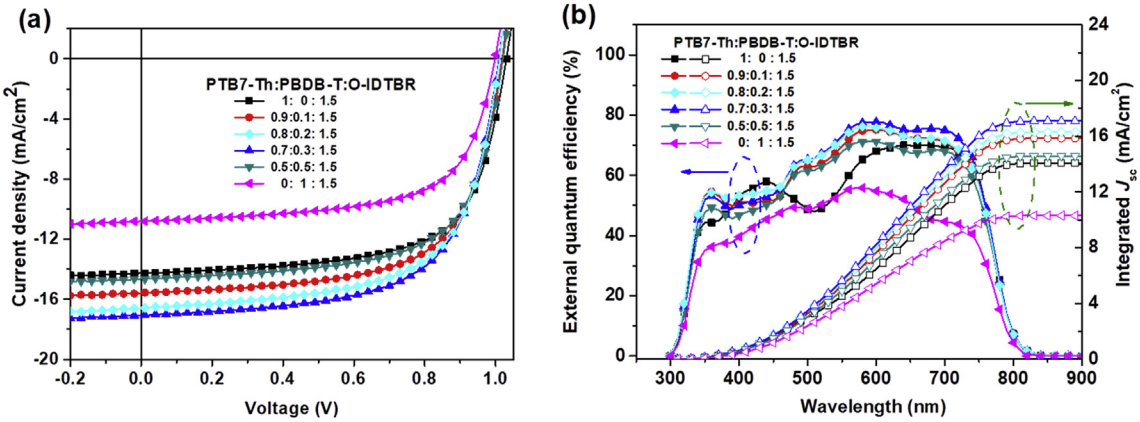

Fig. 2. (a) *J-V* characteristics and (b) EQE curves of the PSCs based on PTB7-Th:PBDB-T:O-IDTBR with different weight ratios of PBDB-T in the polymer donor. The integrations of the EQE curves for J_{sc} are also shown.

Table 1
The photovoltaic performance parameters of the binary and ternary PSCs at different contents of PBDB-T in the polymer donor under AM1.5G illumination at 100 mW cm^{-2}.

PTB7-Th:PBDB-T:O-IDTBR	V_{oc}	J_{sc}	J_{cal}	FF	PCE
	[V]	[mA cm^{-2}]	[mA cm^{-2}]	[%]	[%] (ave.)[a]
1:0:1.5	1.03	14.25	14.07	66.38	9.74 (9.62)
0.9:0.1:1.5	1.02	16.13	15.85	63.84	10.59 (10.21)
0.8:0.2:1.5	1.02	16.58	16.29	64.81	10.96 (10.39)
0.7:0.3:1.5	1.02	17.07	17.09	66.52	11.58 (11.23)
0.5:0.5:1.5	1.01	14.62	14.59	65.97	9.81 (9.71)
0:1:1.5	1.00	10.80	10.28	64.79	6.99 (6.72)

[a] Average values in the parentheses are based on 10 devices.

device structure of ITO/PEODT:PSS/active layer/PFN-Br/Al, where ITO is indium tin oxide, PEDOT:PSS is poly(3,4-ethylenedioxythiophene):poly(styrene-sulfonate), and PFN-Br is poly[(9,9-bis(3'-((*N*,*N*-dimethyl)-*N*-ethylammonium)-propyl)-2,7-fluorene)-alt-2,7-(9,9-dioctylfluorene)] [52]. The weight ratio of polymer donor and O-IDTBR acceptor was kept at 1:1.5 in this study. The active layers (~100 nm) were spin-coated with *o*-dichlorobenzene solutions, with 0.5% 1-chloronaphthalene (1-CN) as the solvent additive. Annealing temperature of 120 °C for 10 min was applied for the active layers. The optimizations for the annealing temperature and the 1-CN content are given in Tables S2 and S3 in the Supporting Information. Fig. 2a shows the current density-voltage (*J-V*) characteristics of the PSCs with the PBDB-T contents of 0%, 10%, 20%, 30%, 50%, and 100% in the polymer donors. The photovoltaic parameters of the binary and ternary PSCs are summarized in Table 1.

The binary reference device based on PTB7-Th:O-IDTBR showed a maximum PCE of 9.74%, based on V_{oc} of 1.03 V, J_{sc} of 14.25 mA cm^{-2}, and FF of 66.38%. The efficiency is comparable with that for the PTB7-Th:O-IDTBR active layer in a previous report by Rath et al. [53]. It should be noted that the high V_{oc} of 1.03 eV for the PTB7-Th:O-IDTBR based PSCs implies very low energy loss (E_{loss}). In terms of an empirical formula, E_{loss} equals to the lowest energy bandgap $E_{g\text{-}opt}$ minus eV_{oc}, i.e. $E_{loss} = E_{g\text{-}opt} - eV_{oc}$. Based on the $E_{g\text{-}opt}$ of 1.52 eV for O-IDTBR, the E_{loss} is as low as 0.49 eV. With the addition of 10% PBDB-T for a ternary system, the PCE of the solar cell was improved to 10.59% due to almost unchanged V_{oc} of 1.02 V, obviously higher J_{sc} of 16.13 mA cm^{-2}, and slightly decreased FF of 63.84%. With higher PBDB-T contents of 20% and 30%, the J_{sc} values of devices could be elevated to 16.58 and 17.07 mA cm^{-2}, and the FF values were improved to 64.81% and 66.52%, respectively. As a result, continuously increased PCEs of 10.96% and 11.58% were found. Further increasing PBDB-T content to 50%, the ternary devices showed a lower PCE of 9.81%, mainly due to the decreased J_{sc} of 14.62 mA cm^{-2}. For the PBDB-T:O-IDTBR binary PSCs, further decreased J_{sc} of 10.80 mA cm^{-2} was found. The binary devices displayed the lowest photovoltaic performances (PCE = 6.99%), despite fairly high V_{oc} of 1 V and FF of 64.79%. In general, the selection of the two polymer donors with comparable E_{HOMO} is useful to achieve 2D/1A ternary PSCs with high and the ternary active layers with PBDB-T contents between 10% and 30% can also show much better photovoltaic performances if compared with the two binary PSCs.

Since the HOMO level of PBDB-T is lower-lying than that of PTB7-Th, normally the V_{oc} of a PBDB-T based PSC should be higher than that of a PTB7-Th based device when paring a same acceptor. In previous reports with a fullerene acceptor, the PBDB-T and PTB7-Th based PSCs displayed V_{oc} values of 0.86 and 0.80 V, respectively [55,56]. When nonfullerene ITIC was used as the acceptor, the PBDB-T based device also gave a higher V_{oc} of 0.90 V if compared with a V_{oc} of 0.81 for the PTB7-Th [57,58]. It should be noted that, relative to the 1.03 V for the PTB7-Th:O-IDTBR system, the PBDB-T:O-IDTBR binary PSCs with a lower V_{oc} of 1 V is abnormal. The reason for this behavior is still unknown, which needs more systematic study on the energy loss factors. For the PTB7-Th:PBDB-T:O-IDTBR ternary system, the PSCs with higher PBDB-T contents also show a decreasing tendency of the V_{oc}, confirming the decreasing V_{oc} effect by the PBDB-T. Consequently, the PBDB-T:O-IDTBR binary PSCs exhibit the largest E_{loss} of 0.52 eV.

The EQE spectra of the binary and ternary PSCs are shown in Fig. 2b. For the reference binary device based on PTB7-Th:O-IDTBR, its EQE curve showed strong spectral responses from 600 to 730 nm but weak responses around 520 nm. The integrated current density (J_{cal}) for the EQE curve is 14.07 mA cm^{-2}, showing a very small spectral mismatch of 1.3%. The EQE behavior of the binary PSC can somewhat correspond to the absorption spectrum of the PTB7-Th:O-IDTBR blend film as shown in Fig. 1d. For the PTB7-Th:PBDB-T:O-IDTBR ternary active layers with PBDB-T contents from 10% to 50%, the relatively weak spectral response region of the PTB7-Th:O-IDTBR binary active

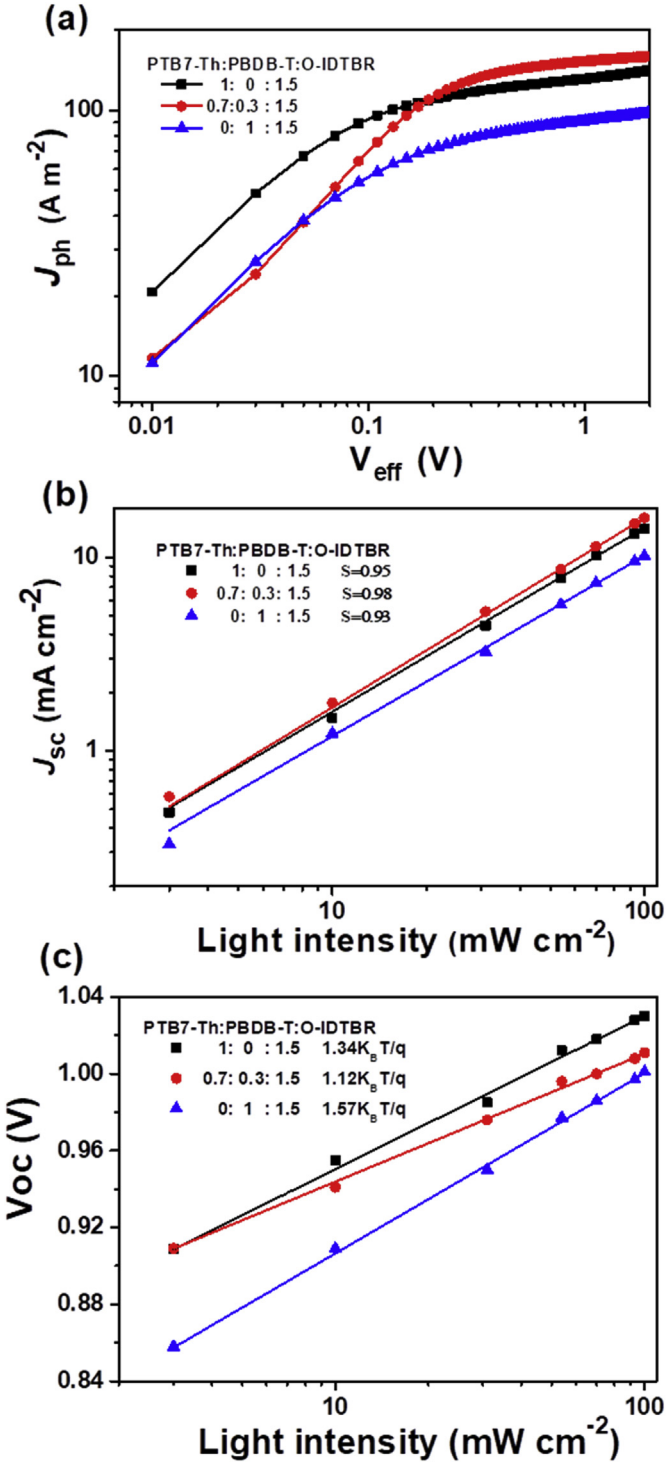

Fig. 3. (a) Photocurrent density versus effective voltage characteristics, (b) dependence of J_{sc} on light intensity, and (c) dependence of V_{oc} on light intensity for the PTB7-Th:O-IDTBR, PTB7-Th:PBDB-T:O-IDTBR (0.7:0.3:1.5), PBDB-T:O-IDTBR devices.

layer could be enhanced obviously, in which the PTB7-Th:PBDB-T:O-IDTBR = 0.7:0.3:1.5 displayed the highest EQE of 77% at ~600 nm. Continuously enhanced J_{cal} values from 15.85 to 16.29 and then to 17.09 mA cm^{-2} were found for ternary active layers with PBDB-T contents from 10% to 20% and then 30%, well correlating those of 16.13, 16.58, and 17.07 mA cm^{-2} achieved in the *J-V* measurements. The spectral mismatches are all less than 2%. For a higher PBDB-T content of 50%, the ternary PSC exhibited weakened spectral responses from 350 to 500 nm, resulting in a J_{cal} of 14.59 mA cm^{-2}, almost identical to the J_{sc} achieved in the *J-V* measurement. The binary PSC based on PBDB-T:O-IDTBR showed the lowest spectral response, with a maximum EQE of only 56%. Its J_{cal} is 10.28 mA cm^{-2}, showing a larger mismatch of 5%.

To gain more insight into light absorption and the exciton dissociation process, we determined the saturation current density J_{sat} and charge dissociation probabilities P(E,T) of PTB7-Th:O-IDTBR, PTB7-Th:PBDB-T:O-IDTBR (0.7:0.3:1.5), PBDB-T:O-IDTBR devices. Fig. 3a presents photocurrent density (J_{ph}) versus effective voltage (V_{eff}) curves for the PSCs used in this work. Here, J_{ph} can be gained by subtracting the dark current from the current under illumination and V_{eff} can be gained by subtracting the applied voltage from the voltage where J_{ph} is zero [30]. If we assume that all the photogenerated excitons are dissociated into free charge carriers and collected by electrodes at a high V_{eff} (that is, V_{eff} = 2 V), the J_{sat} will only be limited by maximum exciton generation rate (G_{max}) [59]. As a result, $J_{sat} = qLG_{max}$, where q is elementary charge and L is the thickness of active layer. The G_{max} values for the three devices were 8.85 × 10^{27} for the PTB7-Th:O-IDTBR loading with J_{sat} = 153.6 A m^{-2}, 1.05 × 10^{28} for the PTB7-Th:PBDB-T:O-IDTBR loading with J_{sat} = 179.8 A m^{-2}, and 7.00 × 10^{27} m^{-3} s^{-1} for the PBDB-T:O-IDTBR loading with J_{sat} = 120.3 A m^{-2}. For the ternary device, the highest G_{max} suggests the best overall exciton generations. This should be ascribed to the absorption contribution of PBDB-T, from which exciton harvesting of the PTB7-Th:PBDB-T:O-IDTBR ternary blend film in wavelength range from 320 to 635 nm can be obviously enhanced if compared with PTB7-Th:O-IDTBR binary blend film. The P(E,T) is determined from the ratio of J_{ph}/J_{sat}. The P(E,T) values at short circuit condition for the PTB7-Th:O-IDTBR, PTB7-Th:PBDB-T:O-IDTBR (0.7:0.3:1.5), PBDB-T:O-IDTBR devices were 92.73%, 94.95%, and 89.74%, respectively. The results show that the incorporation of PBDB-T can facilitate exciton dissociation in the ternary devices. Therefore, the cascade alignment for the LUMO levels of the ternary blend should play very positive effect on the exciton dissociation if compared with the two binary blends.

The dependences of J_{sc} and V_{oc} at various light intensities can offer deeper insight into the influence of PBDB-T on recombination process in our ternary system. The relationship between J_{sc} and light intensity (P) can be described by the formula of $J_{sc} \propto P^S$. If all free carriers are swept out and collected at the electrodes prior to recombination, the S should be equal to 1, while S < 1 indicates existing of biomolecular recombination [59]. Fig. 3b illustrates J_{sc} as a function of P for the PTB7-Th:O-IDTBR, PTB7-Th:PBDB-T:O-IDTBR (0.7:0.3:1.5), PBDB-T:O-IDTBR devices. The extracted S values are 0.95, 0.98, and 0.93 for three devices, respectively. The results demonstrate that the ternary PSC shows the lowest extent of biomolecular recombination. Fig. 3c shows the relationship between V_{oc} and P in our PSCs. The slope of V_{oc} versus log(P) helps us to determine the degree of trap-assisted recombination in the devices. A slope at k_BT/q implies that bimolecular recombination is the dominating mechanism, where k_B is Boltzmann's constant, T is absolute temperature and q is elementary charge. As for trap-assisted or Shockley-Read-Hall recombination, a stronger dependence of V_{oc} on light intensity with a slope of 2 k_BT/q is observed [59]. In our cases, the PTB7-Th:O-IDTBR and PBDB-T:O-IDTBR binary devices showed the slopes of 1.34 and 1.57 k_BT/q while for the PTB7-Th:PBDB-T:O-IDTBR ternary device, a relatively small slope of 1.12 k_BT/q was attained. The results indicate that addition of PBDB-T into the PTB7-Th:O-IDTBR blend can reduce interfacial surface trap densities and suppress trap-assisted recombination, giving an enhanced J_{sc}.

Space-charge-limited current (SCLC) method was performed for the binary and ternary blend films to better understand their charge transport property. The structures of electron-only and hole-only devices are ITO/ZnO/active layer/PFN-Br/Al and ITO/PEDOT:PSS/Active layer/MoO_3/Al [31,60], respectively, and the relevant SCLC curves are shown in Fig. S2. The electron mobilities (μ_e) for the PTB7-Th:O-IDTBR and PBDB-T:O-IDTBR blend films are comparable of 5.19 × 10^{-4} and

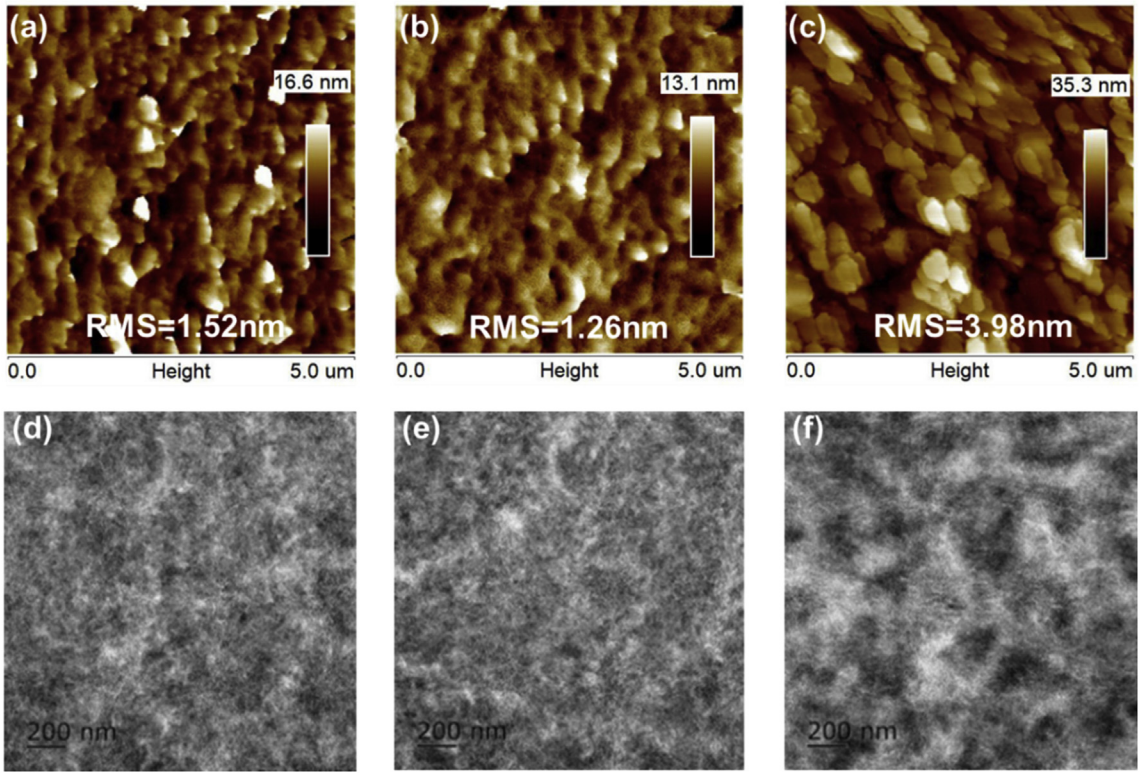

Fig. 4. (a–c) AFM height images and (d–f) TEM images for (a,d) PTB7-Th:O-IDTBR, (b,e) PTB7-Th:PBDB-T:O-IDTBR (0.7:0.3:1.5), and (c,f) PBDB-T:O-IDTBR blend films.

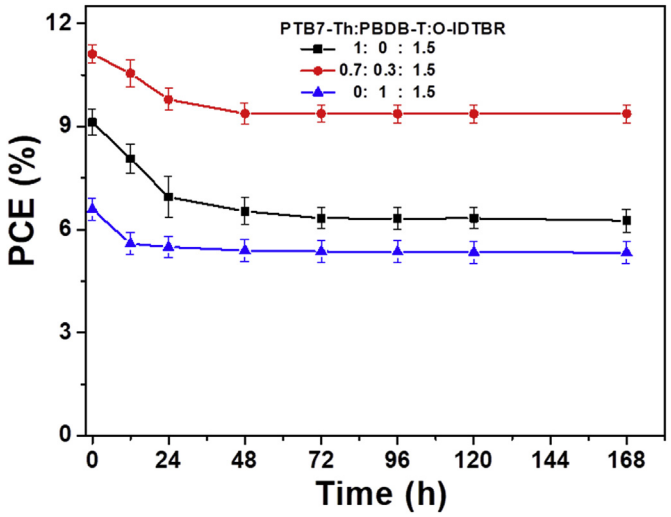

Fig. 5. PCEs of the PSC devices after long-term annealing at 85 °C in N_2 glove box.

4.85×10^{-4} $cm^2/(V\ s)$, respectively. Relatively, the PTB7-Th:PBDB-T:O-IDTBR (0.7:0.3:1.5) blend film can show a higher μ_e of 6.59×10^{-4} $cm^2/(V\ s)$, suggesting a better continuity of the acceptor phase in the BHJ blend film. For the hole-only devices, the PTB7-Th:O-IDTBR and PBDB-T:O-IDTBR blend films also display very close hole mobilities (μ_h) of 8.78×10^{-4} and 8.08×10^{-4} $cm^2/(V\ s)$, respectively. For the PTB7-Th:PBDB-T:O-IDTBR (0.7:0.3:1.5) blend film, an enhanced μ_h of 1.45×10^{-3} $cm^2/(V\ s)$ can be achieved. The results suggest that the hole transport barrier in-between the two polymer donors is very small, which can be ascribed to the comparable E_{HOMO} values for PTB7-Th and PBDB-T. The calculated μ_h/μ_e values for the binary and ternary blend films are between 1.67 and 2.20, indicating fairly balanced carrier transport. This has been reflected by the very close FF between 64.79% and 66.52% for the three PSCs.

To study the influence of PBDB-T on the morphology of the films of the ternary blends, atomic force microscopy (AFM) measurements and transmission electron microscopy (TEM) were performed. As shown in Fig. 4, the thin PTB7-Th:O-IDTBR exhibited a surface with a root-mean-square (RMS) roughness value of 1.52 nm. After adding 30% PBDB-T, the ternary blend film exhibited a more uniform morphology and smooth surface with RMS value of 1.26 nm. This may have resulted from the good miscibility between PTB7-Th and PBDB-T, as they both have a benzodithiophene (BDT) in their molecule structures. However, the thin PBDB-T:O-IDTBR film have a much larger RMS value of 3.98 nm probably due to the high crystallinity of the PBDB-T, which maybe a non-negligible reason for the lower J_{sc} and PCE of the resulting devices. From the TEM images, the ternary blend film showed more obvious and better phase separation than the PTB7-Th:O-IDTBR and PBDB-T:O-IDTBR blend films, which can be beneficial for excitons separation and charge transportation. Furthermore, some fine dispersed fibrils could be observed in the ternary blend films when the content of PBDB-T was incorporated, which provided more high-speed channels for charge transportation.

The stability of a solar cell under thermal stress is an essential consideration for the practical application. In this regard, we compared the thermal stability of PTB7-Th:O-IDTBR, PTB7-Th:PBDB-T:O-IDTBR (0.7:0.3:1.5) and PBDB-T:O-IDTBR based devices (Fig. 5). The thermal annealing was conducted at 85 °C in the N_2 glove box up to a long period of 168 h. For the PTB7-Th:O-IDTBR based binary PSCs, the annealing during the initial 24 h showed obvious PCE drops, and then the efficiency decreased very slowly up to 72 h. Thereafter, PCEs $\geq$6.27% could be kept after the 168 h annealing. The PBDB-T:O-IDTBR based devices could show a faint PCE drop after the initial 24 h annealing. However, the PSCs could only display PCEs of 5.33% after the 168 h annealing due to the not high original efficiency of the binary active layer. Relatively, the PTB7-Th:PBDB-T:O-IDTBR based ternary PSCs

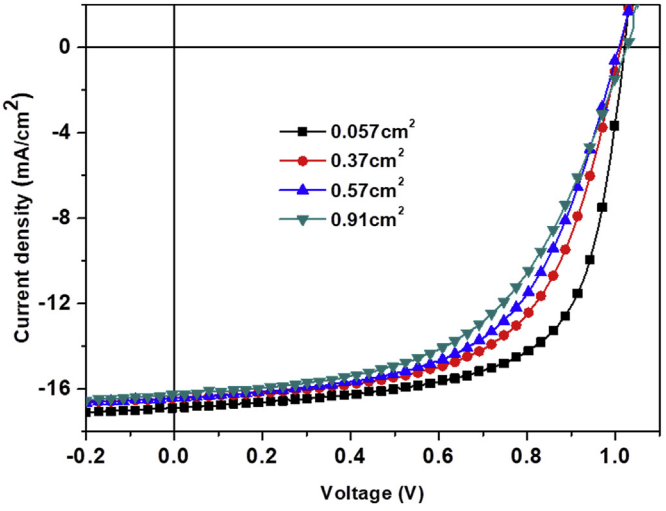

Fig. 6. *J-V* characteristics of the ternary PSCs with different device areas, based on PTB7-Th:PBDB-T:O-IDTBR = 0.7:0.3:1.5.

could keep a high level of efficiency. After the initial 48 h annealing, the PSCs could show nearly unchanged efficiency. The final PCEs for the devices were 9.37% after the 168 h annealing. The results demonstrate the good thermal stability of the ternary blend films, which can not only achieve a high initial efficiency but also keep it at a high level after a long-term thermal annealing.

It is worth pointing out that all of the above-mentioned devices have an area of 0.057 cm^2. With the PTB7-Th:PBDB-T:O-IDTBR (0.7:0.3:1.5) ternary blend as the active layer, we also evaluated the photovoltaic performances of larger area devices of 0.37, 0.57, and 0.91 cm^2 (Fig. 6). So far, experimental data for PSCs with large area of ~1 cm^2 are extremely scarce [61,62]. The detailed photovoltaic parameters are listed in Table S4. The larger area devices of 0.37, 0.57, and 0.91 cm^2 exhibited PCEs of 10.12%, 9.51%, and 9.01%, respectively. With increasing of the device area, the PSCs with different device areas showed almost identical V_{oc} and only slightly decreased J_{sc}. However, continuously dropped FF could be found and the 0.91 cm^2 device only remained a FF of 54.18%. With increasing of the device area, the ternary PSCs exhibited obviously increased series resistance (R_s) and the decreased shunt resistance (R_{sh}) (Table S4), which resulted in the decreasing of FF.

3. Conclusions

In summary, high V_{oc} nonfullerene ternary PSCs were designed based on O-IDTBR acceptor and two compatible polymer donors of PTB7-Th and PBDB-T with comparable HOMO levels. The V_{oc} of 1.02 V for the ternary PSCs is one of the highest values among 2D/1A ternary devices. A maximum PCE of 11.58% could be achieved for the ternary PSCs based on PTB7-Th:PBDB-T:O-IDTBR (0.7:0.3:1.5) blend film, significantly higher than 9.74% and 6.99% for PTB7-Th:O-IDTBR and PBDB-T:O-IDTBR binary blend film, respectively. The improved efficiency with the ternary PSCs was due to the significantly elevated J_{sc}, which was confirmed by the obviously enhanced EQE and charge dissociation probabilities. In addition, the ternary blend film also displayed the highest mobilities for both hole and electron as well as favorable morphology. More importantly, the ternary solar cells also exhibited much higher efficiency after a long thermal annealing if compared with the two binary devices. Large area ternary devices were evaluated and a PCE of 9.01% was achieved for device area of 0.91 cm^2. Our results demonstrated a high V_{oc} strategy for ternary PSCs, in which the efficiency and thermal stability could be optimized.

Notes

The authors declare no competing financial interest.

Acknowledgement

The authors thank the financial support of National Natural Science Foundation of China (U1401244, 51521002, 91633301, 21225418), National Basic Research Program of China (973 program 2013CB834705), and Natural Science Foundation of Guangdong Province (2016A030312002).

Appendix A. Supplementary data

Supplementary data to this article can be found online at https://doi.org/10.1016/j.orgel.2019.03.030.

References

[1] G. Li, R. Zhu, Y. Yang, Polymer solar cells, Nat. Photon. 6 (2012) 153–161.
[2] M.A. Green, K. Emery, Y. Hishikawa, W. Warta, E.D. Dunlop, Solar cell efficiency tables, Prog. Photovoltaics 24 (2016) 3–11.
[3] L. Lu, T. Xu, W. Chen, E.S. Landry, L. Yu, Ternary blend polymer solar cells with enhanced power conversion efficiency, Nat. Photon. 8 (2014) 716–722.
[4] F.C. Krebs, N. Espinosa, M. Hösel, R.R. Søndergaard, M. Jørgensen, 25th Anniversary article: rise to power-OPV-based solar parks, Adv. Mater. 26 (2014) 29–39.
[5] Y.-W. Su, S.-C. Lan, K.-H. Wei, Organic photovoltaics, Mater. Today 15 (2012) 554–562.
[6] P. Sonar, J.P.F. Lim, K.L. Chan, Organic non-fullerene acceptors for organic photovoltaics, Energy Environ. Sci. 4 (2011) 1558–1574.
[7] X. Ma, W. Gao, J. Yu, Q. An, M. Zhang, Z. Hu, J. Wang, W. Tang, C. Yang, F. Zhang, Ternary nonfullerene polymer solar cells with efficiency > 13.7% by integrating the advantages of the materials and two binary cells, Energy Environ. Sci. 11 (2018) 2134–2141.
[8] X. Liu, B. Xie, C. Duan, Z. Wang, B. Fan, K. Zhang, B. Lin, F.J. Colberts, W. Ma, R.A. Janssen, F. Huang, Y. Cao, A high dielectric constant non-fullerene acceptor for efficient bulk-heterojunction organic solar cells, J. Mater. Chem. A 6 (2018) 395–403.
[9] Q. Fan, W. Su, Y. Wang, B. Guo, Y. Jiang, X. Guo, F. Liu, T.P. Russell, M. Zhang, Y. Li, Synergistic effect of fluorination on both donor and acceptor materials for high performance non-fullerene polymer solar cells with 13.5% efficiency, Sci. China Chem. 61 (2018) 531–537.
[10] W. Liu, J. Zhang, Z. Zhou, D. Zhang, Y. Zhang, S. Xu, X. Zhu, Design of a new fused-ring electron acceptor with excellent compatibility to wide-bandgap polymer donors for high-performance organic photovoltaics, Adv. Mater. 30 (2018) 1800403.
[11] Z. Fei, F.D. Eisner, X. Jiao, M. Azzouzi, J.A. Röhr, Y. Han, M. Shahid, A.S. Chesman, C.D. Easton, C.R. McNeill, T.D. Anthpopulos, J. Nelson, M. Heeney, An alkylated indacenodithieno [3,2-*b*] thiophene-based nonfullerene acceptor with high crystallinity exhibiting single junction solar cell efficiencies greater than 13% with low voltage losses, Adv. Mater. 30 (2018) 1705209.
[12] W. Wang, B. Zhao, Z. Cong, Y. Xie, H. Wu, Q. Liang, S. Liu, F. Liu, C. Gao, H. Wu, Y. Cao, Nonfullerene polymer solar cells based on a main-chain twisted low-bandgap acceptor with power conversion efficiency of 13.2%, ACS Energy Lett. 3 (2018) 1499–1507.
[13] D. Yan, W. Liu, J. Yao, C. Zhan, Fused-ring nonfullerene acceptor forming interpenetrating J-architecture for fullerene-free polymer solar cells, Adv. Energy Mater. 8 (2018) 1800204.
[14] Z. Luo, C. Sun, S. Chen, Z.-G. Zhang, K. Wu, B. Qiu, C. Yang, Y. Li, C. Yang, Side-chain impact on molecular orientation of organic semiconductor acceptors: high performance nonfullerene polymer solar cells with thick active layer over 400 nm, Adv. Energy Mater. 8 (2018) 1800856.
[15] X. Song, N. Gasparini, L. Ye, H. Yao, J. Hou, H. Ade, D. Baran, Controlling blend morphology for ultrahigh current density in nonfullerene acceptor-based organic solar cells, ACS Energy Lett. 3 (2018) 669–676.
[16] X. Song, N. Gasparini, M.M. Nahid, H. Chen, S.M. Macphee, W. Zhang, V. Norman, C. Zhu, D. Bryant, H. Ade, I. McCulloch, D. Baran, A highly crystalline fused-ring n-type small molecule for non-fullerene acceptor based organic solar cells and field-effect transistors, Adv. Funct. Mater. 28 (2018) 1802895.
[17] W. Zhao, S. Li, H. Yao, S. Zhang, Y. Zhang, B. Yang, J. Hou, Molecular optimization enables over 13% efficiency in organic solar cells, J. Am. Chem. Soc. 139 (2017) 7148–7151.
[18] Q. An, W. Gao, F. Zhang, J. Wang, M. Zhang, K. Wu, X. Ma, Z. Hu, C. Jiao, C. Yang, Energy level modulation of non-fullerene acceptors enables efficient organic solar cells with small energy loss, J. Mater. Chem. A 6 (2018) 2468–2475.
[19] N.A. Ran, J.A. Love, C.J. Takacs, A. Sadhanala, J.K. Beavers, S.D. Collins, Y. Huang, M. Wang, R.H. Friend, G.C. Bazan, T.-Q. Nguyen, Harvesting the full potential of photons with organic solar cells, Adv. Mater. 28 (2016) 1482–1488.
[20] H. Zhang, H. Yao, J. Hou, J. Zhu, J. Zhang, W. Li, R. Yu, B. Gao, S. Zhang, J. Hou, Over 14% efficiency in organic solar cells enabled by chlorinated nonfullerene

small-molecule acceptors, Adv. Mater. 30 (2018) 1800613.
[21] S. Li, L. Ye, W. Zhao, H. Yan, B. Yang, D. Liu, W. Li, H. Ade, J. Hou, A wide band gap polymer with a deep highest occupied molecular orbital level enables 14.2% efficiency in polymer solar cells, J. Am. Chem. Soc. 140 (2018) 7159–7167.
[22] H. Li, Z. Xiao, L. Ding, J. Wang, Thermostable single-junction organic solar cells with a power conversion efficiency of 14.62%, Sci. Bull. 63 (2018) 340–342.
[23] B. Kan, H. Feng, H. Yao, M. Chang, X. Wan, C. Li, J. Hou, Y. Chen, A chlorinated low-bandgap small-molecule acceptor for organic solar cells with 14.1% efficiency and low energy loss, Sci. China Chem. 61 (2018) 1307–1313.
[24] R.A. Janssen, J. Nelson, Factors limiting device efficiency in organic photovoltaics, Adv. Mater. 25 (2013) 1847–1858.
[25] A. Polman, M. Knight, E.C. Garnett, B. Ehrler, W.C. Sinke, Photovoltaic materials: present efficiencies and future challenges, Science 352 (2016) aad4424.
[26] P. Heremans, D. Cheyns, B.P. Rand, Strategies for increasing the efficiency of heterojunction organic solar cells: material selection and device architecture, Accounts Chem. Res. 42 (2009) 1740–1747.
[27] L. Nian, Y. Kan, H. Wang, K. Gao, B. Xu, Q. Rong, R. Wang, J. Wang, F. Liu, J. Chen, G. Zhou, T.P. Russell, A.K.-Y. Jen, Ternary non-fullerene polymer solar cells with 13.51% efficiency and a record-high fill factor of 78.13%, Energy Environ. Sci. 11 (2018) 3392–3399.
[28] M. Zhang, W. Gao, F. Zhang, Y. Mi, W. Wang, Q. An, J. Wang, X. Ma, J. Miao, Z. Hu, X. Liu, J. Zhang, C. Yang, Efficient ternary non-fullerene polymer solar cells with PCE of 11.92% and FF of 76.5%, Energy Environ. Sci. 11 (2018) 841–849.
[29] L. Zhong, H. Bin, Y. Li, M. Zhang, J. Xu, X. Li, H. Huang, Q. Hu, Z.-Q. Jiang, J. Wang, C. Zhang, F. Liu, T.P. Russell, Z. Zhang, Y. Li, Ternary non-fullerene polymer solar cells with a high crystallinity n-type organic semiconductor as the second acceptor, J. Mater. Chem. A 6 (2018) 24814–24822.
[30] Z. Wang, H. Jiang, L. Zhang, X. Liu, J. Sun, Y. Cao, J. Chen, 1D/2A ternary blend active layer enables as-cast polymer solar cells with higher efficiency, better thickness tolerance, and higher thermal stability, Org. Electron. 61 (2018) 359–365.
[31] X. Liu, Y. Yan, Y. Yao, Z. Liang, Ternary blend strategy for achieving high-efficiency organic solar cells with nonfullerene acceptors involved, Adv. Funct. Mater. 28 (2018) 1802004.
[32] X. Song, N. Gasparini, M.M. Nahid, S.H.K. Paleti, J.-L. Wang, H. Ade, D. Baran, Dual sensitizer and processing-aid behavior of donor enables efficient ternary organic solar cells, Joule (2019), https://doi.org/10.1016/j. joule. 2019.01.009.
[33] Z. Cai, D. Zhao, V. Sharapov, M.A. Awais, N. Zhang, W. Chen, L. Yu, Enhancement in open-circuit voltage in organic solar cells by using ladder-type nonfullerene acceptors, ACS Appl. Mater. Interfaces 10 (2018) 13528–13533.
[34] Y. Xie, Y. Yu, Q. Liang, J.-H. Wan, H. Wu, Y. Cao, Understanding the enhanced open-circuit voltage of polymer solar cells based on a diketopyrrolopyrrole small molecular acceptor, ACS Appl. Mater. Interfaces 10 (2018) 25589–25593.
[35] Y. Yang, J. Wang, H. Xu, X. Zhan, X. Chen, Nonfullerene acceptor with “donor–acceptor combined π-bridge” for organic photovoltaics with large open-circuit voltage, ACS Appl. Mater. Interfaces 10 (2018) 18984–18992.
[36] B. Xiao, A. Tang, J. Zhang, A. Mahmood, Z. Wei, E. Zhou, Achievement of high V_{oc} of 1.02 V for P3HT-based organic solar cell using a benzotriazole-containing nonfullerene acceptor, Adv. Energy Mater. 7 (2017) 1602269.
[37] D. Baran, T. Kirchartz, S. Wheeler, S. Dimitrov, M. Abdelsamie, J. Gorman, R.S. Ashraf, S. Holliday, A. Wadsworth, N. Gasparini, P. Kaienburg, H. Yan, A. Amassian, C.J. Brabec, J.R. Durrant, I. McCulloch, Reduced voltage losses yield 10% efficient fullerene free organic solar cells with > 1 V open circuit voltages, Energy Environ. Sci. 9 (2016) 3783–3793.
[38] S. Chen, Y. Liu, L. Zhang, P.C. Chow, Z. Wang, G. Zhang, W. Ma, H. Yan, A wide-bandgap donor polymer for highly efficient non-fullerene organic solar cells with a small voltage loss, J. Am. Chem. Soc. 139 (2017) 6298–6301.
[39] W. Ni, M. Li, B. Kan, F. Liu, X. Wan, Q. Zhang, H. Zhang, T.P. Russell, Y. Chen, Fullerene-free small molecule organic solar cells with a high open circuit voltage of 1.15 V, Chem. Commun. 52 (2016) 465–468.
[40] X. Liu, X. Du, J. Wang, C. Duan, X. Tang, T. Heumueller, G. Liu, Y. Li, Z. Wang, J. Wang, F. Liu, N. Li, C.J. Brabec, F. Huang, Y. Cao, Efficient organic solar cells with extremely high open-circuit voltages and low voltage losses by suppressing nonradiative recombination losses, Adv. Energy Mater. 8 (2018) 1801699.
[41] D. Yang, Y. Wang, T. Sano, F. Gao, H. Sasabe, J. Kido, A minimal non-radiative recombination loss for efficient non-fullerene all-small-molecule organic solar cells with a low energy loss of 0.54 eV and high open-circuit voltage of 1.15 V, J. Mater. Chem. A 6 (2018) 13918–13924.
[42] X. Xu, Z. Li, W. Zhang, X. Meng, X. Zou, D. Di Carlo Rasi, W. Ma, A. Yartsev, M.R. Andersson, R.A. Janssen, E. Wang, 8.0% efficient all-polymer solar cells with high photovoltage of 1.1 V and internal quantum efficiency near unity, Adv. Energy Mater. 8 (2018) 1700908.
[43] D. Baran, R.S. Ashraf, D.A. Hanifi, M. Abdelsamie, N. Gasparini, J.A. Röhr, S. Holliday, A. Wadsworth, S. Lockett, M. Neophytou, C.J.M. Emmott, J. Nelson, C.J. Braabec, A. Amassian, A. Salleo, T. Kirchartz, J.R. Durrant, I. McCulloch, Reducing the efficiency-stability-cost gap of organic photovoltaics with highly efficient and stable small molecule acceptor ternary solar cells, Nat. Mater. 16 (2017) 363–369.
[44] Z. Hu, F. Zhang, Q. An, M. Zhang, X. Ma, J. Wang, J. Zhang, J. Wang, Ternary nonfullerene polymer solar cells with a power conversion efficiency of 11.6% by inheriting the advantages of binary cells, ACS Energy Lett. 3 (2018) 555–561.
[45] L. Xiao, T. Liang, K. Gao, T. Lai, X. Chen, F. Liu, T.P. Russell, F. Huang, X. Peng, Y. Cao, Ternary solar cells based on two small molecule donors with same conjugated backbone: the role of good miscibility and hole relay process, ACS Appl. Mater. Interfaces 9 (2017) 29917–29923.
[46] Y.-Y. Yu, T.-W. Tsai, C.-P. Chen, Efficient ternary organic photovoltaics using two conjugated polymers and a nonfullerene acceptor with complementary absorption and cascade energy-level alignment, J. Phys. Chem. C 122 (2018) 24585–24591.
[47] X. Liao, F. Wu, L. Chen, Y. Chen, Crystallization and optical compensation by fluorinated rod liquid crystals for ternary organic solar cells, J. Phys. Chem. C 120 (2016) 18462–18472.
[48] L. Ye, H.-H. Xu, H. Yu, W.-Y. Xu, H. Li, H. Wang, N. Zhao, J.-B. Xu, Ternary bulk heterojunction photovoltaic cells composed of small molecule donor additive as cascade material, J. Phys. Chem. C 118 (2014) 20094–20099.
[49] D. Tang, J. Wan, X. Xu, Y.W. Lee, H.Y. Woo, K. Feng, Q. Peng, Naphthobistriazole-based wide bandgap donor polymers for efficient non-fullerene organic solar cells: significant fine-tuning absorption and energy level by backbone fluorination, Nanomater. Energy 53 (2018) 258–269.
[50] P. Bi, T. Xiao, X. Yang, M. Niu, Z. Wen, K. Zhang, W. Qin, S.K. So, G. Lu, X. Hao, Regulating the vertical phase distribution by fullerene-derivative in high performance ternary organic solar cells, Nano energy 46 (2018) 81–90.
[51] S. Zhang, L. Ye, W. Zhao, D. Liu, H. Yao, J. Hou, Side chain selection for designing highly efficient photovoltaic polymers with 2D-conjugated structure, Macromolecules 47 (2014) 4653–4659.
[52] K. Zhang, Z. Hu, R. Xu, X.F. Jiang, H.L. Yip, F. Huang, Y. Cao, High-performance polymer solar cells with electrostatic layer-by-layer self-assembled conjugated polyelectrolytes as the cathode interlayer, Adv. Mater. 27 (2015) 3607–3613.
[53] S.F. Hoefler, T. Rath, N. Pastukhova, E. Pavlica, D. Scheunemann, S. Wilken, B. Kunert, R. Resel, M. Hobisch, S. Xiao, G. Bratina, G. Trimmel, The effect of polymer molecular weight on the performance of PTB7-Th:O-IDTBR non-fullerene organic solar cells, J. Mater. Chem. A 6 (2018) 9506–9516.
[54] S. Wu, Polar and nonpolar interactions in adhesion, J. Adhes. 5 (1973) 39–55.
[55] D. Qian, L. Ye, M. Zhang, Y. Liang, L. Li, Y. Huang, X. Guo, S. Zhang, Z. Tan, J. Hou, Design, Application and morphology study of a new photovoltaic polymer with strong aggregation in solution state, Macromolecules 45 (2012) 9611–9617.
[56] L. Zhao, S. Zhao, Z. Xu, B. Qiao, D. Huang, X. Xu, Two effects of 1,8-diiodooctane on PTB7-Th:$PC_{71}BM$ polymer solar cells, Org. Electron 34 (2016) 188–192.
[57] W. Zhao, D. Qian, S. Zhang, S. Li, O. Inganas, F. Gao, J. Hou, Fullerene-free polymer solar cells with over 11% efficiency and excellent thermal stability, Adv. Mater. 28 (2016) 4734–4739.
[58] Y. Lin, J. Wang, Z.G. Zhang, H. Bai, Y. Li, D. Zhu, X. Zhan, An electron acceptor challenging fullerenes for efficient polymer solar cells, Adv. Mater. 27 (2015) 1170–1174.
[59] L. Lu, W. Chen, T. Xu, L. Yu, High-performance ternary blend polymer solar cells involving both energy transfer and hole relay processes, Nat. Commun. 6 (2015) 7327.
[60] X. Liu, L. Nian, K. Gao, L. Zhang, L. Qing, Z. Wang, L. Ying, Z. Xie, Y. Ma, Y. Cao, Low band gap conjugated polymers combining siloxane-terminated side chains and alkyl side chains: side-chain engineering achieving a large active layer processing window for PCE > 10% in polymer solar cells, J. Mater. Chem. A 5 (2017) 17619–17631.
[61] B. Fan, X. Du, F. Liu, W. Zhong, L. Ying, R. Xie, X. Tang, K. An, J. Xin, N. Li, W. Ma, C.J. Brabec, F. Huang, Y. Cao, Fine-tuning of the chemical structure of photoactive materials for highly efficient organic photovoltaics, Nat. Energy 3 (2018) 1051–1058.
[62] R. Sun, J. Guo, C. Sun, T. Wang, Z. Luo, Z. Zhang, X. Jiao, W. Tang, C. Yang, Y. Li, J. Min, A universal layer-by-layer solution-processing approach for efficient non-fullerene organic solar cells, Energy Environ. Sci. 12 (2019) 384–395.